Simulation study of poled low-water ionomers with different architectures

2011 J. Phys.: Condens. Matter 23 455102

(http://iopscience.iop.org/0953-8984/23/45/455102)

J. Phys.: Condens. Matter **23** (2011) 455102 (7pp) doi:10.1088/0953-8984/23/45/455102

Simulation study of poled low-water ionomers with different architectures

Elshad Allahyarov[1,2,3], Philip L Taylor[1] and Hartmut Löwen[2]

[1] Department of Physics, Case Western Reserve University, Cleveland, OH 44106, USA
[2] Institut für Theoretische Physik II, Heinrich-Heine Universität Düsseldorf Universitätstrasse 1, 40225 Düsseldorf, Germany
[3] Theoretical Department, Joint Institute for High Temperatures, Russian Academy of Sciences (IVTAN), 13/19 Izhorskaya street, Moscow 125412, Russia

E-mail: elshad.allakhyarov@case.edu

Received 11 August 2011, in final form 15 September 2011
Published 5 October 2011
Online at stacks.iop.org/JPhysCM/23/455102

Abstract
The role of the ionomer architecture in the formation of ordered structures in poled membranes is investigated by molecular dynamics computer simulations. It is shown that the length of the sidechain L_s controls both the areal density of cylindrical aggregates N_c and the diameter of these cylinders in the poled membrane. The backbone segment length L_b tunes the average diameter D_s of cylindrical clusters and the average number of sulfonates N_s in each cluster. A simple empirical formula is noted for the dependence of the number density of induced rod-like aggregates on the sidechain length L_s within the parameter range considered in this study.

(Some figures in this article are in colour only in the electronic version)

1. Introduction

Many ion-exchange membranes are composed of polymers with pendant sidechains attached to the backbone [1]. The most commonly used ionomer, Du Pont's Nafion®, has sidechains ending with the sulfonic acid group SO_3H [2]. When Nafion is hydrated, its sidechain terminal groups dissociate, releasing protons H^+ and leaving the negative groups SO_3^-. As a result of the complex interaction between the hydrophilic and hydrophobic components, the membrane undergoes a nanophase separation [3]. The terminal groups SO_3^- aggregate into clusters, whose shape depends on the membrane's water content, which is characterized by the parameter λ that represents the average number of water molecules per sulfonate group. The clusters are believed to be roughly spherical in low-water-content membranes, but more like fibrils in high-water-content membranes [4, 5]. An interconnection of the clusters into a percolating network is necessary for proton transport through the membrane.

An important goal in the development of new and structurally modified membranes is to design a material that retains an acceptable proton conductivity at low λ. It is known that at the small water contents for which $\lambda < 5$, the water molecules predominantly condense on sulfonates [6], and consequently have a higher boiling and a lower freezing temperature than bulk water. A benefit of low-λ membranes is thus the broad range of their operational temperature [7]. The other advantages of low-λ membranes include their rapid start-up and a reduction in physical degradation of the membrane. The major disadvantage of low-water ionomers is that the undeveloped network of sulfonate clusters has few connecting bridges between clusters. In these ionomers the protons mostly remain within a given cluster until, on a longer time scale, a temporary bridge is formed to the next cluster. An enhancement of the membrane conductivity cannot usefully be achieved by increasing the sulfonate concentration, as this would result in a material of poor mechanical strength and increased solubility [8].

Specific treatments and structural modifications of low-λ ionomers are thus necessary for the formation of a continuous network of hydrophilic clusters. Membranes can, for example, be made that contain particles with functional groups on their surface [9–11], or that contain electro-active particles aligned in one direction [12]. Membrane stretching [13, 14] or the confinement of the polymer in narrow pores [15] also results in an enhanced clustering of sidechains into continuous

pathways. Experimental results on the ordering of Nafion sulfonates into cylindrical aggregates by a strong applied poling field are reported in [16–18]. In our previous work [19, 20], poling-induced reorganization of sulfonate groups into ordered long cylinder-like clusters was observed in molecular dynamics simulations. We reported the self-organization of the terminal groups into cylindrical clusters that resemble the inverted cylinders proposed by Schmidt-Rohr *et al* in [21].

Recent results on Nafion-like ionomers of various composition [22–29] show that short-sidechain membranes have an improved mechanical stability in a broad range of operating temperatures. However, there is still an ongoing debate about the performance of these materials. On the one hand, Arcella *et al* [25] found that the conductivity of Hyflon, a close relative of Nafion, but with shorter sidechains, was higher than that of Nafion. On the other hand, according to Brandell *et al* [30], the mobility of sidechains in Hyflon is less than of that of Nafion. In [30] it is also shown that the sidechains of Aciplex, another modified ionomer with sidechains longer than those of Nafion, have smaller mobility than Nafion. In a previous paper [31] we showed that the increased flexibility of longer sidechains might facilitate proton diffusion.

In the current study we investigate how ionomer structural parameters, such as the sidechain and backbone segment lengths, determine the geometry of the ordered phase in poled and low-water membranes. This extends our earlier work [31] on unpoled membranes, where we showed that the size and sulfonate population of hydrophilic clusters depend strongly on the backbone and sidechain length parameters. In particular, we demonstrated the crucial role of longer sidechains in leading to the formation of larger clusters with a high sulfonate content. Here we analyze the dependence of the number, diameter and population of induced rod-like clusters on the ionomer structure of the poled material.

The rest of the paper is organized as follows. In section 2 we briefly describe the main features of our coarse-grained model. The case of poled membranes with the same sidechain lengths but different backbone segment lengths, known as homologous ionomers, is considered in section 3. An analogous case of membranes with the same backbone segments but different sidechains is considered in section 4. In section 5 we analyze the morphological differences between two membranes with an equal equivalent weight (EW) but different sidechain and backbone segments. In section 6 a simple empirical formula is noted for the dependence of the number density of induced aggregates on the sidechain length. The anisotropic nature of the ion diffusion in poled structures is studied in section 7, and we conclude in section 8.

2. Coarse-graining and system parameters

Fully atomistic simulations of hydrated ionomers are, for practical reasons, generally limited to simulation cells of only a few nanometers in length. They can thus be used to study small-scale phenomena such as the swelling of single clusters, the conformational dynamics of a few sidechains, or the proton diffusion in simple pores, but cannot readily be used to investigate morphology on a scale larger than that of single clusters. An investigation of more complex problems, such as the large-scale morphological changes induced by strong perturbing fields, demands a coarse-grained treatment of the polymer structure. Usually the simulated ionomer is coarse-grained into chains of beads interacting through model-specific force field potentials. There are three principal coarse-graining levels encountered in the theory of ionomer simulations. In the framework of the first, the lowest-level coarse-graining approach, the entire sidechain and large segments of the backbone are replaced by giant beads. This approach is mostly employed in dissipative particle dynamics simulations [28, 32]. While very large systems can be investigated using such an extreme approximation, it comes at the cost of losing any information about the proton diffusion in the predicted morphologies. Within the second, middle-level coarse-graining, typically between two and four CF_x groups of the polymer are combined into single beads. Although this approach is adequate for the prediction of the membrane morphology [27], it nevertheless still fails in its description of ion dynamics in clusters. Here we confine ourselves to the highest-level coarse-graining approach, which invokes the united-atom model [33, 13, 20, 34, 22, 35–37]. In the framework of this model, the structural geometry of the coarse-grained ionomer is defined by the number L_b of repeat units of CF_2 in the hydrophobic backbone, and the total number L_s of repeat units of CF_2, CF_3, ether oxygen, and hydrophilic terminal group monomers of the sidechain. The two end monomers of the sidechain are the sulfur atom and the oxygen group O_3. The number of sulfonates m in the simulation cell of volume $V = L^3$ sets the concentration of sulfonates η (mol l^{-1}), and is related to the equivalent weight of the membrane, defined as the mass of ionomer in grams per mole of sulfonate ions.

We consider five different ionomer architectures corresponding to the combinations of L_b and L_s [31][4] given in figure 1. The sequence B, C, D in this figure corresponds to a gradual increase in the backbone segment length L_b, while keeping the sidechain length L_s constant. Along this sequence the number of sulfonates m in the simulation cell decreases, and thus the membrane EW increases from 1170 to 1840. The pair C, E involves an increase in L_s at constant L_b. Finally, along the sequence D, E, F, the membrane architecture is changed from a short L_s and a long L_b to a long L_s and a short L_b membrane. This change is made at a fixed EW by keeping the sum $L_s + L_b$ constant.

The united-atom units are modeled as Lennard-Jones (LJ) monomers with size $\sigma = 0.35$ nm [13, 19, 20]. All hydrophobic monomers are treated as electrostatically neutral, the electrostatic charges being located entirely on the hydrophilic SO_3^- sulfonate head groups, and on the H^+

[4] We omit the analysis of membrane A with $L_s = L_b = 8$, which was considered in a previous publication [31]. The ordered structure of sulfonates in this membrane appears to be unstable against thermal fluctuations, and reverts back to the structure of the unpoled membrane after the poling field is removed.

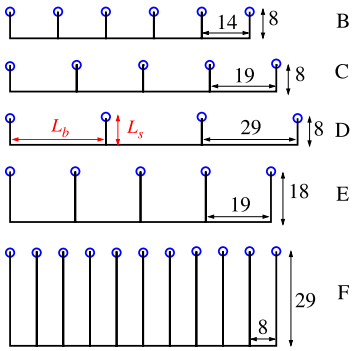

Figure 1. Schematic representation of ionomers with different sidechain lengths L_s and backbone segment lengths L_b. The segment lengths are given in numbers of united-atom monomers. Along the sequence B, C, D, the backbone segment length L_b increases at constant sidechain length L_s. Along this sequence the polymer EW is increased from 1170 to 1840. Along the sequence D, E, F, the sidechain length L_s is increased at constant $L_s + L_b$, and thus at a constant EW.

protons[5]. The corresponding charges are $+1.1e$ for the sulfur atom, $-2.1e$ for the combined oxygens O_3, and $+1.0e$ for the proton.

A modified force field, based on the classical Dreiding force field [38], was used in our united-atom model, full details of which are given in [31]. The water is modeled as a TIP3P liquid [39]. We fixed the water content parameter $\lambda = 3$ for all simulation runs. The TIP3P explicit charges $q_H = +0.417e$ and $q_O = -2q_H$ are placed on the hydrogen and oxygen atoms of the water molecule, respectively. The oxygen atom acts as the mass center of the water molecule. The rigid-water model has no geometric flexibility, with the distance between hydrogen and oxygen atoms being $r_{OH} = 0.0957$ nm, and the angle θ_{HOH} between hydrogen bonds being equal to 104.52°. The dipole moment of such a water molecule is 2.35 D. The TIP3P model does not allow for inclusion of the non-classical Grotthuss transport of protons, but this omission does not significantly affect simulation results for ionomers with a low water content.

The simulations were performed in stages. The first step was to grow a continuous backbone with attached pendant sidechains by using Monte–Carlo techniques. The bond length and the bending and dihedral angles for this initial polymer were initially constrained to be their known equilibrium values[6]. Molecular dynamics (MD) runs of 100 ps were used to equilibrate this system by letting it respond to the strong steric repulsion between overlapping monomers. The rigidity constraints on angles and bonds were then removed. The side chains were detached from the backbone skeleton, and the backbone skeleton itself was cut into segments [40, 20, 41]. This procedure greatly increases the relaxation rate of the ionomer, and allowed a rapid equilibration of the short-chain system, which then consisted of m sidechain and m backbone segments.

[5] The H^+ protons in our model are not distinguishable from H_3O^+ hydronium ions, which are usually considered as counterions of sulfonic acids, see [30].

[6] The angle ϕ_0 is equal to π for sidechains and $\pm 2\pi/3$ for backbones.

Molecular dynamics runs with a Langevin thermostat having a friction coefficient $\gamma = 2$ ps^{-1} and a Gaussian white-noise force of strength $6k_BT\gamma$ were performed for the segmented polymer for time periods up to 100 ps in a constant-NVT ensemble. The equations of motion were integrated using the velocity Verlet algorithm with a time step of 0.25 fs. We imposed standard periodic boundary conditions for a cube of side $L = 11.2$ nm by filling space with translational replicas of the fundamental cell. The long-range electrostatic interactions between charged particles were handled using the standard Lekner summation algorithm [42, 43]. In order to verify that the system had not become trapped into a metastable glassy state, we repeated each run from several different initial configurations.

In the next stage of the simulations, the segments were reassembled back into the single branched chain characterizing the original Nafion, in order to avoid introducing spurious effects due to the presence of an unrealistic number of chain ends. This was achieved by the simultaneous introduction of the bonds and angular potentials from the force field [31] between the ends of each backbone segment. This united them into a single chain. Similar bond and angular forces between the tail monomer of each detached side chain and the median monomer of every backbone segment connected the side chains to the backbone polymer. To avoid the formation of star-like branched polymers, only a single occupancy of the backbone attachment sites was permitted. The equal numbers of backbone segments and side chain segments resulted in the formation of a polymer in which there were equal numbers of backbone monomers between the points of attachment of the side chains. The simulation was then resumed under the imposed external electric field along its z-direction. This poling field acted on the head-group monomers of the side chains, on the water molecules, and on the protons in the membrane. During the following 5–10 ns, a new membrane morphology was generally observed to form. This morphology gradually reached a steady state, as monitored by the calculation of the potential energy of the ionomer. Once the drift currents of protons and water molecules through the membrane had stabilized, we gathered statistics during the next 5 ns.

In the third series of simulations, we removed the poling E-field from the membrane and ran the simulations until the entire system reached a new equilibrium. Relaxation from the field-maintained morphology to a new field-free equilibrium appeared rapid, typically taking only a couple of nanoseconds. Then, during the following 5 ns, we investigated the statistical and dynamical properties of the relaxed, poled ionomer. The equilibration was verified by examining the velocity distributions of ions and water, and by the convergence of different parts of the potential energy and of the pair distribution functions of ions, water, and sulfonates. Once the system was fully equilibrated, the statistically averaged quantities necessary to characterize the morphology and proton diffusion were gathered during the next 6 ns of run time at 100 fs intervals.

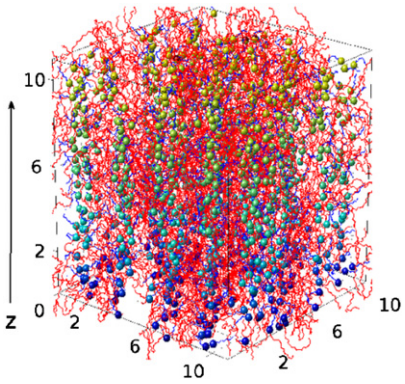

Figure 2. A typical snapshot of the membrane D under a strong poling field along the z axis. The spheres represent the end-group oxygen atoms O_3 of sidechains. The backbone is drawn in red, and the sidechains are drawn in blue (both are dark in grayscale). The colors of the spheres represent altitudes, with a blue (dark in grayscale) used for low-altitude beads (at the bottom of the simulation box) and a yellow (gray in grayscale) used for high-altitude beads (at the top of the simulation box). The size of all structural elements is schematic rather than space filling. The protons and water molecules are not shown for the sake of clarity. The axis distances are given in nanometers.

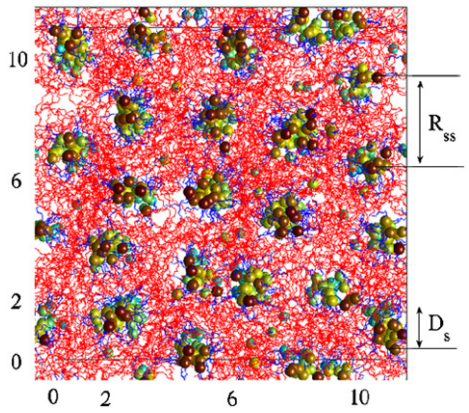

Figure 3. A top (xy) view of the poled membrane D. The color-scale and line notations are the same as in figure 2. Cylindrical clusters of diameter D_s form a hexatic structure with a lattice constant R_{ss}. The axis distances are given in nanometers.

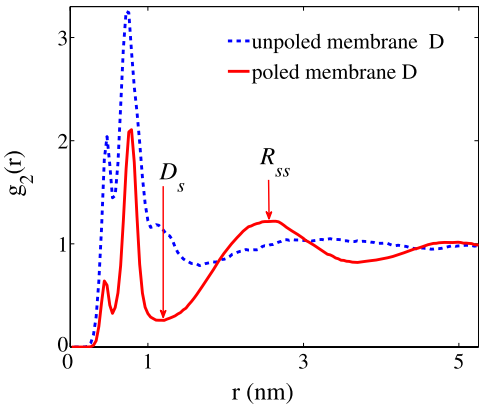

Figure 4. The two-dimensional sulfonate–sulfonate pair correlation function $g_2(r)$ in the xy plane for the poled and unpoled membranes D. In the poled membrane the cluster size D_s is defined as the position of the first minimum after the major multiplet peaks; the cluster–cluster nearest-neighbor distance is defined as the position of the maximum R_{ss} on the right of D_s.

3. Poled membranes with constant L_s and different L_b

Using the procedure described above, we investigated the morphological changes occurring in poled membranes of the homologous series along the sequence B, C, D. Under the poling field, the sulfonate dipoles tend to orient parallel to the z axis of the simulation box, and form a wire-like network of dipoles [20, 19]. At sufficiently strong fields, these wire-like clusters group into longer cylinders along the poling direction. A typical snapshot of this induced morphology is shown in figure 2. When the poling field is released, and the membrane relaxes back to equilibrium, hereafter referred to as the poled state, the induced structure does not completely disappear. The remnant structure of the poled state appears to be thermodynamically favorable compared to the isotropic structure of the unpoled membrane [20, 19]. The top view of the poled membrane D shown in figure 3 reveals the apparent ordering in the positions of rod-like clusters. The structural dimensions of the ordered phase, such as the approximate diameter D_s of cylindrical clusters, and the nearest-neighbor separation between cylinders R_{ss} can be deduced from the shape of the two-dimensional (2D) sulfonate–sulfonate pair correlation function $g_2(r)$ defined as

$$g_2(r) = \frac{L^3}{\pi r\, \mathrm{d}r\, \sigma} \frac{\mathrm{d}n_s(r)}{m}. \qquad (1)$$

Here $\mathrm{d}n_s(r)$ is the number of sulfur atoms in a cylindrical shell of radius r, thickness $\mathrm{d}r$ and height $\sigma/2$, and containing a sulfur atom at the center of the cylinder, while m is the number of sidechains in the simulation box of volume L^3. The function $g_2(r)$ represents the probability of finding two sulfonate monomers at a separation distance r in the xy plane averaged over the equilibrium trajectory of the simulated system. The 2D pair correlation functions for the unpoled and poled membranes D are plotted in figure 4. In both samples the peaks at short distances $r < 1$ nm arise from the clustering of sulfonates into multiplets, and the position of the highest peak is related to the most probable sulfonate–sulfonate separation r_{ss} projected in the xy plane. Low values of r_{ss} facilitate proton hopping between adjacent sulfonates. At distances larger than the multiplet sizes, the function $g_2(r)$ exhibits a well-defined minimum at $r = D_s$ and a maximum at $r = R_{ss}$ for the poled membrane D. These distances correspond to the diameter of the rod-like clusters[7] and the inter-rod separation distance respectively. The emergence of the third peak at about $r = 5$ nm for the poled membrane D in

[7] The average radius $D_s/2$ of a cylindrical cluster is related to the position of the main peak of $g_2(r)$ at $r < 1$ nm. However, the multiplet peaks also appear at $r < 1$ nm, and thus mask the size effect of the cylindrical aggregates. In such a case the other parameter, the position D_s at which the function $g_2(r)$ has a minimum, can be regarded as the average diameter of cylindrical aggregates in poled membranes.

Table 1. Simulated values for the sulfonate concentration η, and the simulation results for the diameter of the cylindrical clusters D_s in the xy plane, the nearest-neighbor separation distance between cylindrical clusters R_{ss} in the xy plane, the nearest-neighbor separation distance between multiplet sulfonates r_{ss} in the xy plane, the cluster occupancy number N_s, and the proton diffusion coefficients D_z and D_{xy} for the membranes identified in figure 1.

Membrane	B	C	D	E	F
η (mol l^{-1})	1.61	1.26	1.08	1.08	1.08
D_s (nm)	1.35	1.30	1.21	1.52	1.56
R_{ss} (nm)	2.66	2.65	2.64	2.98	3.10
r_{ss} (nm)	0.60	0.64	0.70	0.66	0.55
N_s	64	50	36	49	56
D_z (cm^2 s^{-1})	4.8×10^{-6}	3.4×10^{-6}	2.6×10^{-6}	2.7×10^{-6}	2.8×10^{-6}
D_{xy} (cm^2 s^{-1})	2.5×10^{-6}	2.1×10^{-6}	1.7×10^{-6}	1.8×10^{-6}	1.8×10^{-6}

Table 2. Summarized table of qualitative changes in the morphological structure of the poled membrane as a response to the changes in the ionomer segment parameters L_s and L_b. The '+ (−)' signs indicate the tendency to increase (decrease), and the sign '0' means that no significant changes take place.

Parameters changed	Parameters kept constant	D_s	R_{ss}	r_{ss}	N_s	N_c
L_b+	L_s	−	0	+	−	0
L_s+	L_b	+	+	+	0	−
L_s+, L_b-	$L_s + L_b$	+	+	−	+	−

figure 4 is additional evidence for the positional ordering of the cylindrical aggregates in the lateral direction.

The dependence of the multiplet distance r_{ss} and the structural dimensions D_s and R_{ss} on the sidechain branching density along the sequence B, C, D is given in table 1. On the one hand, a decrease in the sulfonate concentration η or, equivalently, an increase in the length of the backbone segment L_b along the sequence B, C, D has very little effect on the ordering length scale R_{ss}. On the other hand, a decrease of η along the sequence B, C, D results in a radial shrinking of the cylinders, and an increase in the multiplet distance r_{ss}.

The finding that the ordering length R_{ss} in homologous membranes does not depend on L_b means that the number of induced cylindrical aggregates N_c formed in the simulation box is constant along the sequence B, C, D. The parameter N_c can be determined as

$$N_c = m/N_s, \tag{2}$$

where the quantity N_s is the average number of sulfonates per cylinder, and is defined as

$$N_s = \frac{2\pi m}{L^2} \int_0^{D_s/2} g_2(r) r \, dr. \tag{3}$$

For the sequence of poled membranes B, C, and D we found that N_s almost halves from 64 to 36, and $N_c = 21$.

It total, we have shown that the backbone segment length L_b can be used as a tuning parameter for the diameter D_s of cylindrical aggregates, making induced clusters thicker or thinner. However, the parameter L_b, has no effect on the lattice constant R_{ss} of the ordered hexatic phase, or on the number of cylindrical aggregates N_c that are formed. All these dependences are qualitatively described in table 2.

4. Poled membranes with constant L_b and different L_s

In this section we investigate how the sidechain length L_s affects the morphological parameters of the ordered phase in poled membranes with a fixed sidechain branching density. For this purpose, we consider the membranes C and E from figure 1, which have the same L_b but different L_s. Simulation results for the parameters r_{ss}, D_s, and R_{ss}, shown in table 1, reveal that the average sulfonate occupancy N_s (equation (3)), is almost the same for the membranes C and E. In other words, the poling of membranes with the same L_b results in the formation of cylindrical aggregates with the same sulfonate occupancy N_s, regardless of how long the sidechains are. The latter regulates the number N_c of cylinders generated (equation (2)): N_c decreases from 21 for membrane C to 16 for membrane E. Changing L_s also results in changing the diameter of the aggregates: the longer the sidechain, the thicker the aggregate is in the radial direction. All these dependences are qualitatively described in table 2.

5. Poled membranes with constant $L_s + L_b$

In previous sections we compared the morphologies of the ordered structures in poled membranes having different sulfonate concentrations η. The charge neutrality condition imposed on the simulated system, and the constraint of a constant water content λ per sulfonate adopted in this work, imply that the concentrations of protons and water molecules in the various poled membranes were different. This means that the electrostatic screening effects, which regulate the clustering of sulfonates and the response of the membrane to external fields, for the sequence of membranes B, C, D, were not the same.

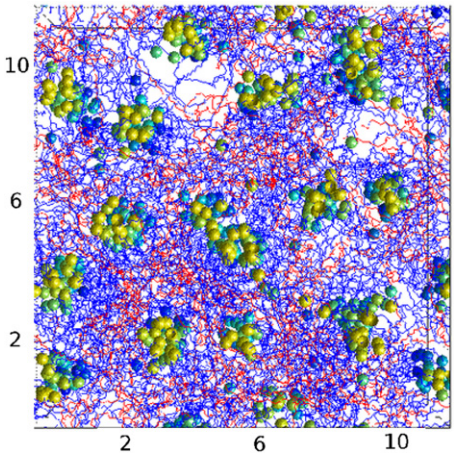

Figure 5. A top (xy) view of the poled membrane F. The color-scale and line notations are the same as in figure 2. The axis distances are given in nanometers.

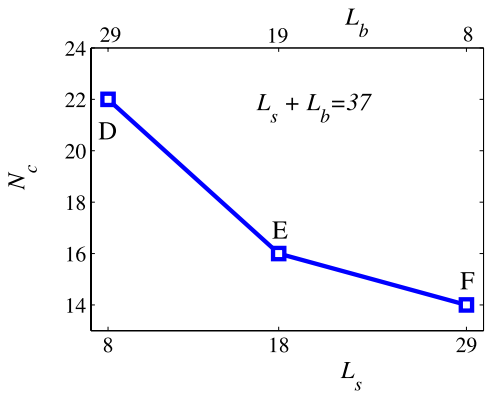

Figure 6. The number of cylindrical clusters N_c for the sequence of membranes D, E, F, with constant $L_s + L_b$ and EW. Note that the increase in L_s is associated with a decrease in L_b, the values of which are shown on the top x axis of the figure.

Thus, in order to escape from the consequences of varying screening effects, and focus on the role the segment lengths L_s and L_b play in the formation of ordered phases, we now consider ionomers with constant $L_s + L_b$, and, therefore, with constant η. We choose the membrane D as a reference membrane with $L_s = 29$ and $L_b = 8$, and consider two of its modifications: a membrane E with $L_s = 18$ and $L_b = 19$, and a membrane F with $L_s = 29$ and $L_b = 8$. The membranes D and F are structural opposites: the L_b and L_s of membrane D correspond to the L_s and L_b of membrane F, respectively.

A visual inspection of the snapshot pictures of the poled membranes D and F, shown in figures 3 and 5 respectively, reveals the existence of strong structural differences between these complementary membranes. Both the cylinder diameter D_s and the inter-cylinder separation distance R_{ss} in membrane F are larger than those in membrane D (see table 1). Overall, the sulfonate population N_s and the structural parameters D_s and R_{ss} increase along the sequence D, E, F. Given that the sulfonate number m is the same for membranes D, E, and F, it is clear, according to equation (2), that an increase in N_s will entail a decrease in the number of cylinders N_c, which is shown in figure 6 as a function of the length L_s.

It total, we found that along the sequence D, E, F, the cylindrical aggregates swell and their number drops from $N_c = 21$ to 14. The swelling of the cylinders is the superposition of two separate swellings originating from the decrease in L_b, considered in section 3, and the increase in L_s, considered in section 4. Along the sequence D, E, F, the multiplet distance r_{ss} decreases, meaning that the influence of the backbone rigidity, at shorter L_b, is much stronger than the effect of the sidechain flexibility, at longer L_s, in the multiplet geometry. All these dependences are qualitatively described in table 2.

6. Phenomenological formula for the number of induced aggregates N_c

We have seen that the number of induced aggregates in poled membranes depends only on the sidechain length L_s, and not on the backbone segment length L_b. The question we now address is whether there is a simple, phenomenological formula that can be used to predict the number of aggregates N_c that would form in the poled membrane.

In the limit of small L_s, the backbone rigidity will prevent the formation of large clusters. The areal density of clusters in a simulation cell, N_c/L^2, will then be large. In the opposite limit where L_s is large, backbone rigidity is unimportant, and the size of clusters will increase until a critical size is reached at which steric factors intervene. Since each hydrophilic end group is attached to a much larger number of hydrophobic units, it becomes physically impossible to find space to insert a new end group within the cluster. We thus expect N_c as a function of L_s to decrease from its initial high level, and then saturate at large L_s (but constant $L_s + L_b$).

Within the limited range we have studied we do not see saturation. Instead, the form of N_c is closely approximated by a function of the form $N_c \propto {L_s}^{-1/3}$. There does not appear to be any physical reason to expect a function of this form at intermediate L_s. It may, however, have some utility as an empirical observation for these materials.

7. Proton diffusion in poled membranes

The proton diffusion in poled membranes is anisotropic, and is more efficient along the cylindrical clusters. The partial self-diffusion coefficients of protons along the poling direction and in the lateral direction were calculated using the Einstein relations

$$D_z = \lim_{t\to\infty} \frac{1}{2} \frac{\mathrm{d}\langle|\vec{z}(t) - \vec{z}(0)|^2\rangle}{\mathrm{d}t}, \qquad D_{xy} = \lim_{t\to\infty} \frac{1}{4} \frac{\mathrm{d}\langle|\vec{r}_{xy}(t) - \vec{r}_{xy}(0)|^2\rangle}{\mathrm{d}t}. \tag{4}$$

Diffusion coefficients found for the ionomers from figure 1 at water content $\lambda = 3$ are given in table 1. As expected, both the D_z and D_{xy} diffusion coefficients show the same dependence on the polymer parameters L_s and L_b as does the multiplet distance r_{ss}. The elongation of the ionomer backbone at constant L_s, or the elongation of the ionomer sidechains at

constant L_b, results in a decrease in proton diffusion. The highest ion diffusion is observed for membrane B, which has the shortest sidechain and backbone segments among the membranes studied. There is a modest increase in proton diffusion D_z for the membranes with constant $L_s + L_b$ when the sidechain length is increased and the backbone length is decreased. This increase appears to be related to the increased flexibility of the longer sidechains.

8. Conclusion

In this paper we have analyzed the role of the structural parameters of ionomers in the formation of the ordered phase in poled membranes. We have found that the sidechain monomeric length L_s effectively controls both the number of cylindrical aggregates N_c and the thickness of these cylinders D_s in the poled membrane. We have noted an empirical formula for N_c which adequately predicts the actual number of induced rod-like cylinders. The significance of this empirical formula lies in the reduced need to perform lengthly simulations on membrane poling in order to determine how many cylindrical clusters will form in a given area of the sample, and in the fact that the sidechain parameter L_s completely defines the number of induced clusters N_c.

We have shown that the backbone segment length L_b can be used to tune both the radius of cylindrical clusters D_s and their population N_s in poled membranes. Bulky cylindrical clusters are formed in membranes with shorter L_b. In a particular case, when the sidechain length is increased at the expense of the backbone segment length, large cylinders with large sulfonate population are grown, in good agreement with the findings of [31]. In this case, the larger the aggregates become, the more they separate from each other, and the closer the sulfonates are in the multiplets. All the structural dependences of the poled state on the ionomer parameters were assembled in table 2.

We note that all our poling molecular dynamics simulations have been performed at room temperature using strong fields. This condition is different from the experimental set-up used by Lin *et al* [16], where membrane poling was carried out for solvent-cast Nafion at elevated temperatures. The decreased viscosity of the polymer in this case makes it possible to use much weaker fields to pole the membrane. Thus, it remains an interesting task to analyze how the ordered phase parameters, such as R_{ss} and D_s, depend on the poling temperature T.

We should also mention that the proton diffusion coefficients presented in table 1 might differ from the hydronium diffusion coefficients that would be measured experimentally in the poled structures considered above. Such a difference might arise from various sources. First, the widely used TIP3P water model does not reproduce the experimental viscosity of water, and thus a specific scaling procedure for the simulated diffusion constants of protons may be needed [44]. Second, the diffusion of hydronium ions in ionomers is affected not only by the type of model used for water, but also by the method of handling hydrogen bonding in the system, the Grotthuss dynamics of hydronium, the form of the ion–water and ion–ion interactions, and the force field parameters used for the polymer material.

Acknowledgments

This work was supported by the US Department of Energy under grant DE-FG02-05ER46244, and was made possible by use of facilities at the Case ITS High Performance Computing Cluster and the Ohio Supercomputing Center. HL thanks the German Science Foundation (DFG) for partial support of this work under grant SFB TR6 (D1).

References

[1] Kreuer K D *et al* 2004 *Chem. Rev.* **104** 4637
[2] Banerjee S and Curtin D E 2004 *J. Fluorine Chem.* **125** 1211
[3] Hsu W Y and Gierke T D 1982 *Macromolecules* **15** 101
Hsu W Y and Gierke T D 1982 *J. Membr. Sci.* **13** 307
[4] Mauritz K A and Moore R B 2004 *Chem. Rev.* **104** 4535
[5] Gebel G and Moore R B 2000 *Macromolecules* **33** 4850
[6] Fimrite J *et al* 2005 *J. Electrochem. Soc.* **152** A1804
[7] Pesaran Y *et al* 2005 *Milestone Report* NREL/MP-540-38760
[8] Hogarth M and Glipa X 2001 *ETSU Technical Report* F/02/00189/REP
[9] Young S K and Mauritz K A 2001 *J. Polym. Sci.* B **39** 1282
[10] Devanathan R 2008 *Energy Environ. Sci.* **1** 101
[11] Alberti G and Casciola M 2003 *Annu. Rev. Mater. Res.* **33** 129
[12] Oren Y *et al* 2004 *J. Membr. Sci.* **239** 17
[13] Allahyarov E and Taylor P 2009 *J. Phys. Chem.* B **113** 610
[14] Lin J *et al* 2007 *Electrochem. Solid-State Lett.* **10** B19
[15] Vorrey S and Teeters D 2003 *Electrochim. Acta* **48** 2137
[16] Lin H L *et al* 2006 *J. Polym. Res.* **13** 379
[17] Middelman E 2002 *Fuel Cell Bull.* **11** 9
[18] Wang Z T 2009 *J. Power Sources* **186** 293
[19] Allahyarov E and Taylor P 2009 *Phys. Rev.* E **80** 020801(R)
[20] Allahyarov E *et al* 2010 *Phys. Rev.* E **81** 031805
[21] Schmidt-Rohr K and Chen Q 2008 *Nature Mater.* **7** 75
[22] Cui S *et al* 2008 *J. Phys. Chem.* B **112** 13273
[23] Paddison S J and Elliott J A 2005 *J. Phys. Chem.* **109** 7583
[24] Paddison S J 2003 *Annu. Rev. Mater. Res.* **33** 289
[25] Arcella V *et al* 2005 *Indust. Eng. Chem. Res.* **44** 7646
[26] Merlo L *et al* 2007 *J. Power Sources* **171** 147
[27] Dorenbos G and Suga Y 2009 *J. Membr. Sci.* **330** 5
[28] Wu D *et al* 2009 *Macromolecules* **42** 3358
[29] Hristov I H *et al* 2008 *J. Phys. Chem.* B **112** 2937
[30] Brandell D 2007 *Mol. Model.* **13** 1039
[31] Allahyarov E and Taylor P 2011 *J. Polym. Sci.* B **49** 368
[32] Malek K *et al* 2008 *J. Chem. Phys.* **129** 204702
[33] Allahyarov E and Taylor P 2007 *J. Chem. Phys.* **127** 154901
[34] Cui S *et al* 2007 *J. Phys. Chem.* B **111** 2208
[35] Vishnyakov A and Neimark A V 2001 *J. Phys. Chem.* B **105** 7830
Vishnyakov A and Neimark A V 2001 *J. Phys. Chem.* B **105** 9586
[36] Yamamoto S *et al* 2004 *14th Int. Conf. on the Properties of Water and Steam, Kyoto* p 411
[37] Jinnouchi R and Okazaki K 2003 *J. Electrochem. Soc.* **150** E66
[38] Mayo S L *et al* 1999 *J. Phys. Chem.* **94** 8897
[39] Mahoney M W and Jorgensen W L 2000 *J. Chem. Phys.* **112** 8910
[40] Glotzer S C and Paul W 2002 *Annu. Rev. Mater. Res.* **32** 401
[41] Vishnyakov A and Neimark A V 2000 *J. Phys. Chem.* B **104** 4471
Rivin D *et al* 2004 *J. Phys. Chem.* B **108** 8900
[42] Lekner J 1989 *Physica* A **157** 826
Lekner J 1991 *Physica* A **176** 485
[43] Mazars M 2001 *J. Chem. Phys.* **115** 2955
[44] Venable R M *et al* 2010 *J. Phys. Chem.* B **114** 12501